Micron 137 (2020) 102910

Contents lists available at ScienceDirect

Micron

journal homepage: www.elsevier.com/locate/micron

Effect of crystallographic orientation on atom probe tomography geochemical data?

Chiara Cappelli*, Alberto Pérez-Huerta

Department of Geological Sciences, The University of Alabama, Tuscaloosa, AL 35487, USA

ARTICLE INFO

Keywords:
Crystallographic orientation
Mass spectrum
Mineral bulk composition
2D density maps
3D spatial reconstruction

ABSTRACT

The recent application of atom probe tomography (APT) to minerals is becoming a powerful tool to unravel geological information from the nanoscale perspective. Yet, there are still unknown fundamental aspects of this microscopy technique for geological applications and the potential crystallographic orientation effect is a significant one. Here, the influence of the crystallographic orientation on the quality of atom probe tomography geochemical data is investigated for two minerals with the same crystal system and different morphology: spinel (isometric, hexoctahedral, octahedron morphology) and galena (isometric, hexoctahedral, cube morphology). Two separate crystals of barite (orthorhombic, dipyramidal, prism morphology) were also analyzed to test the reproducibility of APT data. Despite the general absence of expected stoichiometry, overall bulk and isotopic chemical composition are not affected by crystallographic orientation. 3D data reconstructions of the specimens showed similar spatial distribution of the ion species for each mineral and 2D density maps showed identical (barite, galena) or specular (spinel) patterns for each pair of planes analyzed. Our findings indicate a negligible effect of the crystallographic orientation in APT geochemical data for standard highly symmetric minerals but also suggest the possible influence of the crystallographic structure and composition on the mineral stoichiometry and elements spatial distribution density.

1. Introduction

In the last two decades, micro- and nano-analytical microscopy and geochemical techniques (i.e., secondary ion mass spectrometry (SIMS), transmission electron microscopy (TEM)) have been extensively employed to characterize mineral formation and weathering and link the gathered information to large scale geological phenomena. In this context, atom probe tomography (APT) has become a powerful microscopy technique to investigate a wide range of nanoscale features and processes in minerals (e.g., Pérez-Huerta et al., 2016; Reddy et al., 2020; Saxey et al., 2018). APT provides chemical estimation and 3D analytical mapping of materials at atomic scale offering unique compositional and structural information (Blavette and Sauvage, 2016; Gault et al., 2012; Larson et al., 2013b). Despite many recent improvements on APT (Kelly and Panitz, 2017; Saxey et al., 2018) and the development of commercial laser atom probe system that allows the analysis of non-conductive materials, such as geological samples (Bunton et al., 2007; La Fontaine et al., 2017), there are still factors that can potentially affect the quality of atom probe data. These are in general related to the limitations of the technology behind APT instrumentation (i.e., detector efficiency in local electrode atom probe (LEAP)), sample preparation and running parameters, and data analysis.

A more fundamental factor on which the reliability of the atom probe tomography analysis depends is the intrinsic structure of the sample, specifically its crystallographic structure. In the APT application to the analysis of materials, tip-shaped samples are usually extracted, by focus ion beam (FIB) milling, from a specific crystallographic plane. Ionized atoms evaporated from the tip-specimen are projected onto a detector, and the projection configuration is directly determined by the specimen itself (Larson et al., 2013a). Several studies have recently investigated the effect of crystallography (e.g. crystallographic orientation, crystal plane effect on atomic density variation, stoichiometry vs experimental parameters) in semiconductor materials analysis (aluminium based alloys, De Geuser et al., 2007; GaN nanowires, Diercks et al., 2013; III − N binary and ternary compounds, MgO, and ZnO, Mancini et al., 2014; GaN and AlGaN, Morris et al., 2018; GaN and AlGaN, Morris et al., 2019; GaN, Riley et al., 2012; Fe–C alloys Yao et al., 2010). In particular, De Geuser et al. (2007) analysed two different crystallographic locations [210] and [100] of an aluminium based alloy and found that a correlation in space between evaporated atoms existed and was likely dependent on the crystallographic

* Corresponding author.
E-mail address: ccappelli@ua.edu (C. Cappelli).

https://doi.org/10.1016/j.micron.2020.102910
Received 10 April 2020; Received in revised form 8 June 2020; Accepted 8 June 2020
Available online 12 June 2020
0968-4328/

structure. In fact, there is a general agreement on the existence of preferential evaporation locations, related to both crystal orientation and experimental parameters (especially laser pulse energy), whose presence is due to crystallographic inhomogeneities that show different evaporation field. Depending on the distribution of preferential evaporation locations, events like atomic diffusion and multi-ions evaporation can occur and may lead to bias in local atomic distribution and/or bulk composition possibly affected by atoms loss for pile-up, dead-time effects, and the generation of neutral species (Saxey, 2011).

The crystallographic orientation and matrix effect during *in situ* chemical analysis of mineral samples has already been documented for SIMS spectrometry. Channeling of incident ions and focusing of secondary ions have been identified as possible cause of crystal orientation effects during SIMS analysis of isotopic ratios (oxygen isotope ratio in magnetite, Huberty et al., 2010; oxygen and iron isotope ratios in magnetite Kita et al., 2011; sulfur isotope ratios in sphalerite and galena, Kozdon et al., 2010; $Pb^{206}/^{238}U$ ratios in baddeleyite Wingate and Compston, 2000). These phenomena can take place when the incident angle of the primary ions is parallel to a low-index lattice direction (Kita et al., 2011; Ottolini et al., 2002) and can result in an instrumental bias that leads to an isotope ratio variability which would eventually depend on the crystal structure and orientation (Huberty et al., 2010; Kita et al., 2011). For example, SIMS analysis show no measurable effect on δ18O for a wide range of silicate, carbonate and oxide minerals (Eiler et al., 1997; Śliwiński et al., 2016, 2018; Valley and Kita, 2009) while changes in the instrumental bias lead to oxygen isotope ratio variation for magnetite due to crystal orientation effect (Huberty et al., 2010). In the same way, measurements of oxygen, sulfur and iron isotope ratios in magnetite, sphalerite, and galena show analytical artifacts related to sample tomography and crystal orientation (Kita et al., 2011; Kozdon et al., 2010). On the other hand, analysis of light elements (Li, Be, B, and F) in silicates show that the crystallographic orientation effect is < 10 % relative or below analytical uncertainty in dioctahedral micas (Ottolini et al., 2002). Although, it has been also demonstrated that changes in parameters values (e.g. total impact energy) can improve the analytical precision of isotope ratio measurements (Kozdon et al., 2010).

Also, matrix-dependent elemental fractionation leading to a change in relative proportions of chemical elements has been observed during laser ablation (LA–ICP–MS) analysis (Danyushevsky et al., 2011; Sylvester, 2008). For example, Sylvester (2008) analyzed pyrite, pyrrhotite, chalcopyrite, galena and sphalerite and found that errors for most elements were < 15 % but could raise up to 50 % for some elements (W, Zn and Cd).

Based on the above studies, the potential influence of crystallography structure and crystallographic orientation on the APT analysis of minerals proves to be a factor that needs to be considered in order to gain reliable information about mineral composition and structure (e.g. stoichiometry, preferential element incorporation, presence of sector zoning). In the present study, we focused on the potential effect of crystallographic orientation on atom probe data for two minerals with the same crystal systems and different morphology: spinel (isometric, hexoctahedral, octahedron morphology) and galena (isometric, hexoctahedral, cube morphology). These standard minerals were chosen for their high symmetry and lack of intrinsic anisotropy which avoid the interference of too many factors in the APT analysis (e.g. defects, compositional inhomogeneity, polytypysm). In addition, specimens from the same crystallographic plane of two separate crystal of barite (orthorhombic, dipyramidal, prism morphology) were analyzed to test the reproducibility of APT data and to possibly compare the behavior of some elements (nominally oxygen and sulfur) in different mineral structure. Mass spectra analysis and atomic and isotopic chemical composition estimations were performed to compare APT data sets for each mineral and crystallographic plane analyzed.

2. Methodology

2.1. Materials

Mineral standards, in the form of single crystals of millimetric size, of barite ($BaSO_4$) and galena (PbS) were acquired from SPI Supplies, while a spinel ($MgAl_2O_4$) crystal (catalog no. 112922) was provided by the American Museum of Natural History. The crystals were oriented and selected planes were ultra-polished by sequential grinding, using sandpaper of increasing grit sizes (from 180/P180 to 1200/P2500), and polishing using cloths and Alumina suspension of 0.3 − 0.1 micron (Micropolish II-Buehler). Finally, the samples were rinsed by deionized water, sonicated to eliminate any traces of alumina and dried.

2.2. Methods

2.2.1. Crystallographic plane orientation

Mineral cleavage surfaces, from which tip specimens were extracted, were analyzed by Electron Backscatter Diffraction (EBSD) (coupled to a TESCAN LYRA FIB-FESEM) and/or X-ray diffraction (XRD) (Bruker D8 Discover XRD with GADDS). The (001) crystallographic plane for two separate barite crystals was selected, whereas equivalent (001) and (100) planes and non-equivalent (100) and (111) planes were identified on single crystals of respectively galena and spinel (see Fig. 1).

2.2.2. Focus ion beam (FIB) specimen preparation

Tips of the two selected surfaces of the same crystal for galena and spinel and different crystals for barite were prepared in a dual beam scanning electron microscopy (TESCAN LYRA FIB-FESEM) following a conventional APT sample preparation protocol (Miller et al., 2007). Samples were coated by ~ 20 nm of gold to minimize charging effect during imagining and milling process. A Pt rectangular layer (~3 × 16 μm large and 1 μm high) was deposited on selected areas in order to preserve the surface and reduce Ga^+ implantation during FIB specimen preparation. Milling by Ga^+ ion beam at 30 kV was performed at three side of the Pt layer shaping a specimen wedge (Fig. 2a,b), with a free edge for the attachment of a nanomanipulator (see Gault et al., 2012 and Larson et al., 2013b for more details about FIB specimen preparation protocol). The wedge was then lifted away from the surface and segments of it (~1 − 2 μm) were cut and placed at the top of Si posts of a microtip array coupon (available from CAMECA Scientific Instruments). A sequentially milling by Ga^+ ion beam at 30 and 5 kV was used for tip sharpening in order to obtain a needle-specimen morphology having radius of curvature (half diameter of the top of the tip) ranging from 14 to 48 nm and shank angles between 11° and 46° (Fig. 2c,d).

2.2.3. Local electrode atom probe running and data analysis

Three tip-shaped specimens for each crystallographic orientation and selected crystal for a total of 18 experiments (runs) (Table S1)were analyzed in laser mode (laser wavelength of 355 nm) by a local electrode atom probe (LEAP 5000 XS) with a nominal flight path of 100 nm, housed at the Alabama Analytical Research Center (AARC) of The University of Alabama. The same running parameters were used for each mineral to properly compare data sets (Table S1) and the runs were stopped at ≈20 (barite) and ≈10 (galena, spinel) million ion counts before any specimen fracture. Integrated Visualization and Analysis Software (IVAS 3.8.0) from CAMECA Instrument was used to analyze and reconstruct the data sets. Ions species were defined for each peak of the spectra based on the specific mass-to-charge state ratio and the expected chemical composition. Peaks ranges were manually adjusted taking into account the presence of potential large thermal tails and background levels.

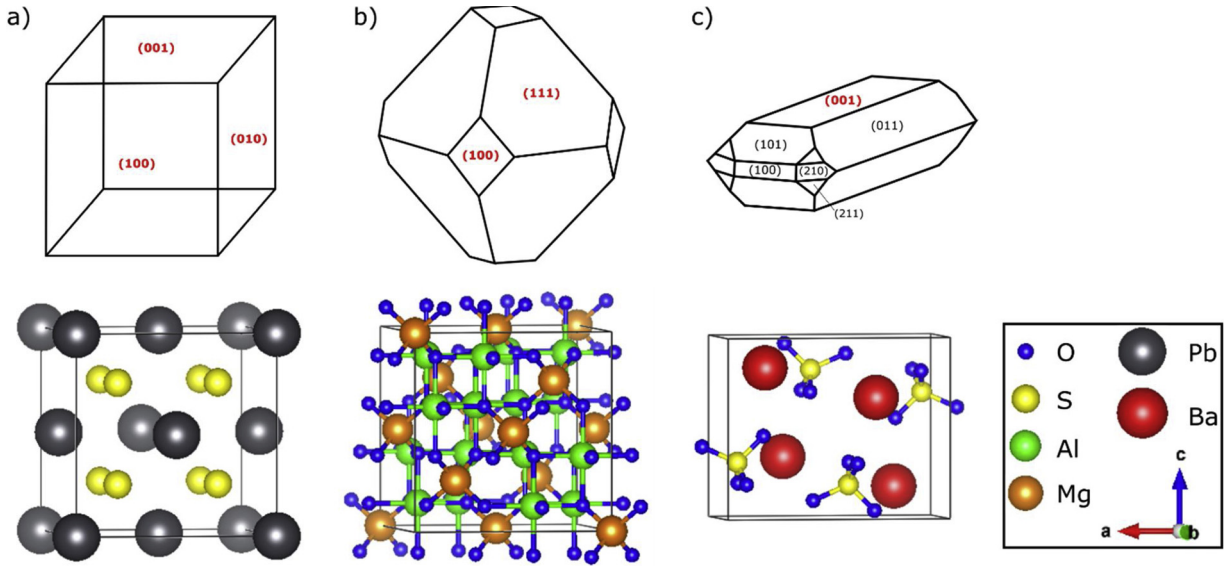

Fig. 1. Schematic of the crystal morphology and structure of a) galena (isometric, hexoctahedral, cube morphology), b) spinel (isometric, hexoctahedral, octahedron morphology) and a) barite (orthorhombic, dipyramidal, prism morphology). In red lettering, the crystallographic indexes of the planes from which the specimen-tips were extracted (Note: For galena, the crystallographic planes are equivalent). (For interpretation of the references to colour in this figure legend, the reader is referred to the web version of this article).

3. Results

3.1. Mass spectra analysis

APT analysis was performed on three specimens for each crystallographic plane and mineral for a total of 18 experiments (runs) (Table S1) and the same number of mass spectra was obtained. The spectra show the ions counts as a function of ion mass-to-charge state ratios defined by the ion time-of-flight measurements (Fig. 3 and Fig. S1). In order to compare mass spectra of different planes for each mineral, ions counts were normalized either to the maximum peak of the spectrum (Ba^{++} for barite, S_2^{+} for galena) or to the peak of the most abundant

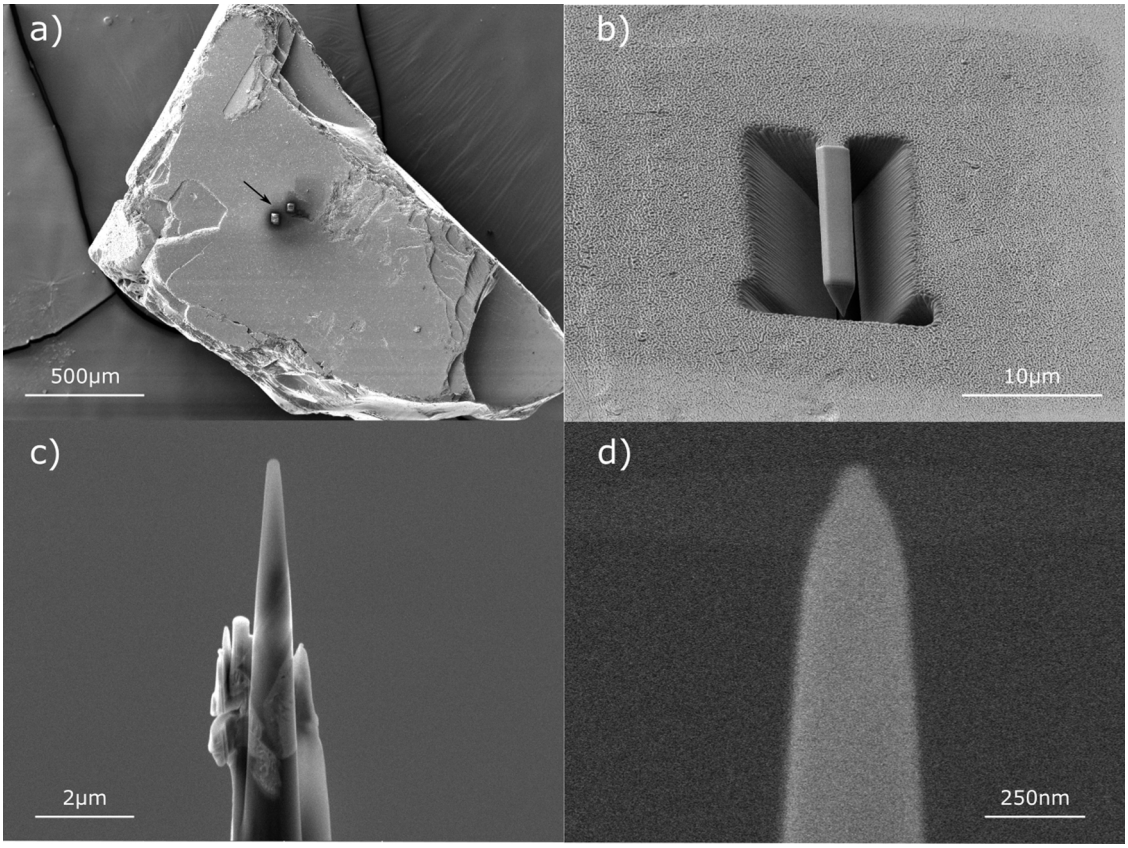

Fig. 2. Examples of SEM images of the lift out process: a) Wedges (black arrow) on barite (001) plane (top view); b) wedge on galena (100) plane (lateral view) after milling at 30 kV; c) and d) spinel tip after 30 kV and 5 kV sharpening, respectively.

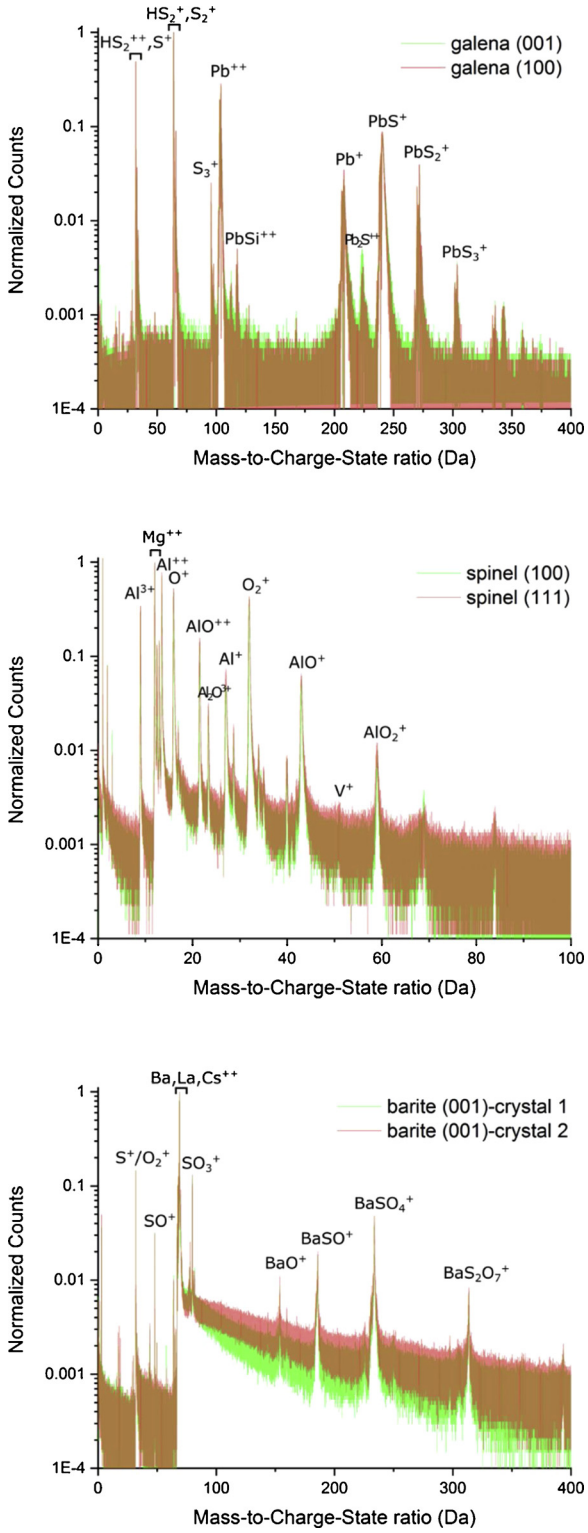

Fig. 3. Comparison of the mass spectra of two tip-specimens extracted from different planes for galena and spinel and the (001) plane of two separate barite crystals. Green and red lines indicate mass spectra of different crystal/crystallographic plane, while brown band indicates the overlapping between the two spectra. Note: in the barite spectrum, the 32 Da peak corresponds to both S + and O_2^+ although it was counted as S^+ for chemical composition estimation according to the sulfur isotopes peaks at 33 and 34 Da. (For interpretation of the references to colour in this figure legend, the reader is referred to the web version of this article).

Table 1
Chemical composition of each crystal/plane and mineral calculated by averaging the data of the three specimens performed for each surface (σ = standard deviation).

Element	Atomic %	σ	Atomic %	σ
	galena (001)		galena (100)	
S	77.27	6.22	79.94	4.91
Pb	22.19	6.43	19.61	4.84
O	0.13	0.05	0.15	0.09
Pt	0.05	0.02	0.09	0.02
Si	0.36	0.20	0.22	0.10
	spinel (100)		spinel (111)	
Si	0.25	0.06	0.20	0.03
Al	28.99	0.27	28.25	0.33
Mg	18.66	0.74	18.75	1.01
O	52.01	0.49	52.71	1.32
V	0.01	0.01	0.01	0.01
Cr	0.06	0.01	0.06	0.00
Na	0.02	0.01	0.02	0.01
	barite (001) crystal 1		barite (001) crystal 2	
S	12.33	0.22	12.15	0.04
Sr	0.15	0.04	0.13	0.03
Ba	53.85	1.78	53.60	0.99
O	31.50	1.37	31.30	0.84
La	0.64	0.08	0.90	0.13
Ce	1.42	0.61	1.81	0.25
Fe	5.0E-03	2.3E-03	4.9E-03	2.4E-04
Ni	0.11	0.02	0.11	0.03

structural ion (Mg^{++} for spinel) in the case of high hydrogen contamination. As shown in Fig. 3a and b, the spectra of the specimens of galena and spinel taken from different crystallographic planes ((001) and (100) for galena; (100) and (111) for spinel) match almost perfectly and all the ranged mass-to-charge ratios (i.e. ion species) were the same for each mineral... Also, no differences were depicted between the spectra of the (001) plane specimens of the two crystals of barite. The apparent difference in the intensity (number of counts) of some peaks (ion species) (Fig. 3) loses its relevance when a carful quantitative analysis of the chemical composition for each specimen of the same crystallographic plane is performed.

3.2. Quantitative chemical data

Table 1 shows the overall chemical composition of the minerals calculated by averaging the results of the APT analysis of the three specimens performed for each crystallographic plane (see also Table S2−4 for the chemical composition of each run). An intrinsic variability is found among specimens with the same orientation due to minor differences in composition and the analytical error associated with each run. In addition, considering the standard deviation, there is no difference observed in the bulk chemical composition for each mineral studied based on the analysis of different crystallographic planes. This is clearly shown by plotting the atomic percentage averages of a crystallographic plane as a function of the averages of the second plane for each mineral. Data match in all cases a 45° slope function (1:1 regression line) within the standard deviation (Fig. 4).

The same general consideration can be made for the analysis of isotopes of each element and each mineral (see Figure S2). Only in a few cases a significant difference was found between the averaged isotopic composition for different planes (see Discussion).

4. Discussion

4.1. Chemical composition

The influence of crystallographic orientation in prior APT analysis of semiconductor materials is difficult to assess. APT works show the crystallographic effect on the compositional analysis for some

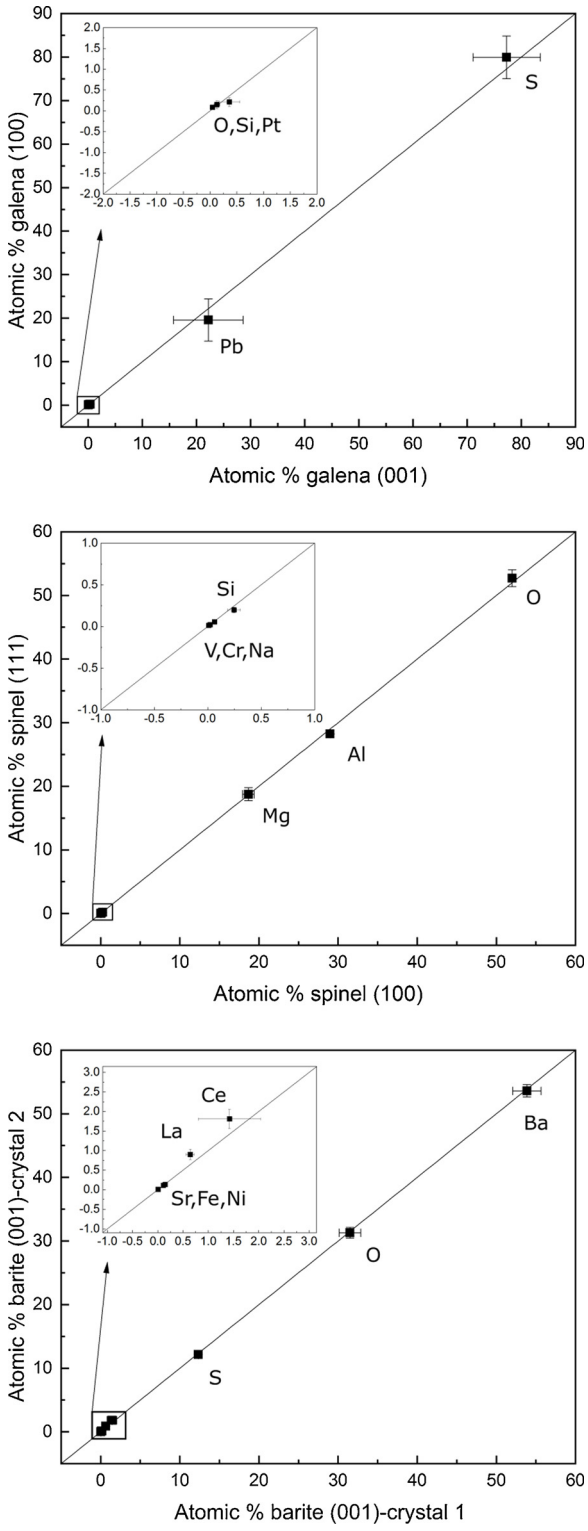

Fig. 4. Plot of the atomic percentage averages of a crystallographic plane as a function of the averages of the second plane for each mineral (see Table 1). The 1:1 regression shows how the results obtained from specimens with different orientation fall apart from each other. Data match in all cases a 1:1 slope function within the standard deviation indicating that no significative difference exists between the compositional estimation of the compared specimens. Note: Black square on the line indicate the zoomed area plotted on the up-left part of each graph.

semiconductor materials (III − N binary and ternary compounds, MgO, and ZnO, Fe-C alloys), but they also point out the strong dependence of the measured element concentrations and distributions on the experimental parameters (Diercks et al., 2013; Morris et al., 2018, 2019; Riley et al., 2012; Yao et al., 2010). The loss in atom detection leading to chemical composition changes would depend on diffusion and multi-ion evaporation events that in turn are affected by the crystallographic structure (Diercks et al., 2013). De Geuser at al. (2007) demonstrated that there is a correlation in space between evaporated atoms due to the existence of preferential evaporation locations. These locations would change with the crystallographic orientation, because of the different variation of the evaporation field on an iso-surface, and over a local area of surrounding neighbors after a single atom evaporation. However, changes on analysis parameters, such as the energy of the laser pulse on which the electric field of the tip depends, can strongly affect the estimation of the chemical composition (Diercks et al., 2013; Mancini et al., 2014; Morris et al., 2018).

In the present study, the same experimental conditions were used for each mineral and crystallographic plane investigated. The APT analysis of galena and spinel have shown not significant effect of the crystallographic orientation on the chemical bulk composition of these minerals (Fig. 3a,b). Neither the bulk composition obtained for the (001) plane specimens of the two samples (crystals) of barite showed important differences (Fig. 3). A minor difference was only observed for the isotope concentration of some elements (V for spinel, Ce for barite, see Fig. S2 and Table S5). Nevertheless, this apparent discrepancy is justified by the higher background that in some spectra does not allow the quantification of ions with very low counts (e.g. V for spinel, Fig. S2c). Big thermal tails of some peaks and overlapping can also interfere in the quantification of minor or trace elements when they have close mass-to-charge state ratios, as for the barium peak (barite) whose thermal tail likely leads to Ce and La concertation underestimation, as these elements have the 138 isotope in common. Although the results are consistent for all minerals and crystallographic planes, the measured atomic percentages do not show stoichiometry. DC-evaporation during the dead time of the detector, the efficiency of the multi-hit events resolution, the loss of neutral desorbed atoms or molecules and the complex decompose analysis of peak overlapping are only some of the reasons explaining the general lack of stoichiometry for APT analysis (Devaraj et al., 2013; Larson et al., 2013b).

Interestingly, same elements but in different minerals showed distinct behavior. For example, the S concentration is very low for a sulphate in barite samples, while it is higher than the stoichiometric value for a sulfide in galena. These two minerals belong to different crystallographic systems (orthorhombic for barite, isometric for galena) and most importantly the sulfur in their structure is differently coordinated and has covalent bonding with oxygens in barite (Ba^{++}—SO_4^{2-}) and ionic bonding with lead in galena (Pb^{++}—S^{2-}) (Fig.1). Also, a lack of oxygen was measured for spinel and even more for barite (Table 1). The O underestimation of APT analysis has already been observed previously, for example, for monazite (Fougerouse et al., 2018), hematite (Bachhav et al., 2013) and apatites (Gordon et al., 2012) and has been ascribed to several possible mechanisms (neutral species evaporation, multi-hit events, dissociation of molecular ions during the flight path, peaks overlapping).

It is worth noting that the experimental parameters have a great influence on both the mass range of the spectrum (type of ions evaporated and detected) and the stoichiometry (percentage of evaporated ions) (Devaraj et al., 2013; Mancini et al., 2014; Morris et al., 2018; Weber et al., 2016). In this regard, a previous APT study on nanostructural features of barite (Weber et al., 2016) documented a variability in the mass range of different specimens and attributed it to the application of different pulse rates. In the same study, the APT spectrum of barite showed, similarly to our results, intense peaks of Ba and a lack of the bulk stoichiometry.

Our findings indicate that an effect of the crystallography structure

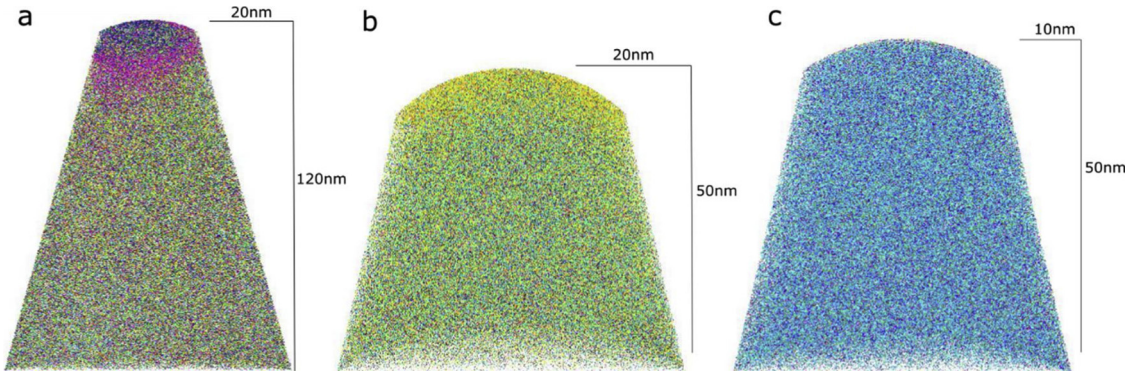

Fig. 5. 3D reconstruction of representative tip-specimen for a) barite, b) galena and c) spinel.

(e.g. orthorhombic vs isometric system) and chemical composition (e.g. sulphate vs sulfide) on the APT data may exist. For this reason, the determination of the best experimetal conditions for the characterization of each mineral by APT is paramout in order to obtain reliable data. In the present study, the main objective was to evaluate the possible effect of the crystallographic orientation on the APT analysis, hence, the same parameters for all the runs were used in order to have as few variables as possible. A rigorous evaluation of the accuracy of the APT on the estimation of the mineral stoichiometry is not the aim of this work and it needs a careful investigation using a sistemic variation of the different experimental parameters.

Nevertheless, the overall absence of stoichiometric values does not influence the assessment of APT data for different crystallographic planes considering the consistency of the data obtained for each mineral studied.

4.2. Atomic distribution: 2D and 3D reconstruction

3D tip reconstruction of the specimens (Fig. 5) show a quite homogenous ions distribution for the three minerals studied, as expected for mainly isotropic and highly symmetric standard mineral samples, and no crystallographic orientation effects were observed in these reconstructions. Only in the case of barite, high concentration of Cs and La is recorded on the top surface of the tip. This morphology is very reproducible over the considered data sets and this finding agrees with the study of Bunney et al. (2014) who observed a preferential substitution of lanthanides along the (001) plane of barite. The preferential elements incorporation into the mineral structure has been object of study since decades for its implication, for example, in geochronology and trace and rare earth elements investigation (Paquette and Reeder, 1995; Reeder and Rakovan, 1999). Based on our observations, APT proves to be a suitable technique for the study of the crystallographic effect on the elements incorporation during crystal growth and possibly of sector zoning. Although, because this is not the object of the present study, we no further addressed this topic.

Recently, some APT studies of semiconductor material have documented a strong influence of the crystal axes on the atomic density distribution and the local stoichiometry s (Diercks et al., 2013; Mancini et al., 2014; Morris et al., 2019; Riley et al., 2012; Yao et al., 2010) and have attributed it to the relation between the electric field distribution on the sample surface and the sample crystallography (Mancini et al., 2014). In these studies, surface areas of different ion density (e.g. pole and line regions) were identified by 2D data reconstruction and cross-sectional analysis. These regions showed different electric field gradients and were associated with the specific specimen crystal planes. For example, low density pole regions would correspond to low order crystallographic planes (major crystallographic directions) and are zones with high electric field gradients between the edges and the center of the pole (Morris et al., 2019; Yao et al., 2010).

In order to evaluate the potential effect of the crystallographic orientation on the distribution of the ion density in our samples, a 2D ion density map for the principle ion species of each mineral and crystal plane (O for spinel, Pb for galena and Ba for barite), was constructed. 2D maps of barite and galena specimens, which were extracted from same and equivalent crystallographic planes respectively, do not show difference of the ion density patterns (Fig. S3). In contrast, the spinel 2D maps show almost specular configurations likely related to the symmetry of the two crystallographic planes analyzed (Fig. 6). Hence, there exists a control of the crystallography itself on the ion density distribution (i.e. pole and line regions). However, this distribution is either the same (barite and galena) or specular (spinel) for each pair of planes analyzed and it does not affect neither the bulk composition nor the spatial reconstruction of the minerals.

5. Conclusions

Atom probe tomography analysis of standard samples of three minerals (barite, galena and spinel) was performed in order to evaluate the effect of the crystal orientation on the quality of APT geochemical data and test its reproducibility. Two different surfaces were selected for each mineral and no significant changes were found in the chemical composition of the bulk for all the studied cases (same, equivalent and non-equivalent crystallographic planes). The mass-to-charge ratio spectra and the atomic percentages were the same, within the standard deviation for each pair of surfaces compared. However, a relationship between mineral crystallography and atom density distribution was observed. Pole and line zones of low density were depicted by 2D density plot of the reconstructed tip-specimens, but the distribution of these zones does not change significantly with the crystal orientation, pointing to the presence of a similar surface electric field pattern for each plane and mineral.

Overall, our findings prove the negligible crystallographic orientation effect on APT geochemical analysis. Yet, our study is based on the analysis of crystals used as standards and minerals with simple crystal morphologies. Thus, our results may not be always applicable to the APT characterization of highly anisotropic minerals and mineral samples whose crystallographic structure is considerably distant from the ideal (i.e. with high density of lattice defects, vacancies, chemical heterogeneities). Further investigation on a wide range of minerals of different crystallographic systems and chemical groups and with structural and compositional heterogeneity is needed in order to abroad our understanding about the effect of the crystallographic orientation on APT mineral characterization.

Declaration of Competing Interest

The authors declare that they have no known competing financial interests or personal relationships that could have appeared to influence the work reported in this paper.

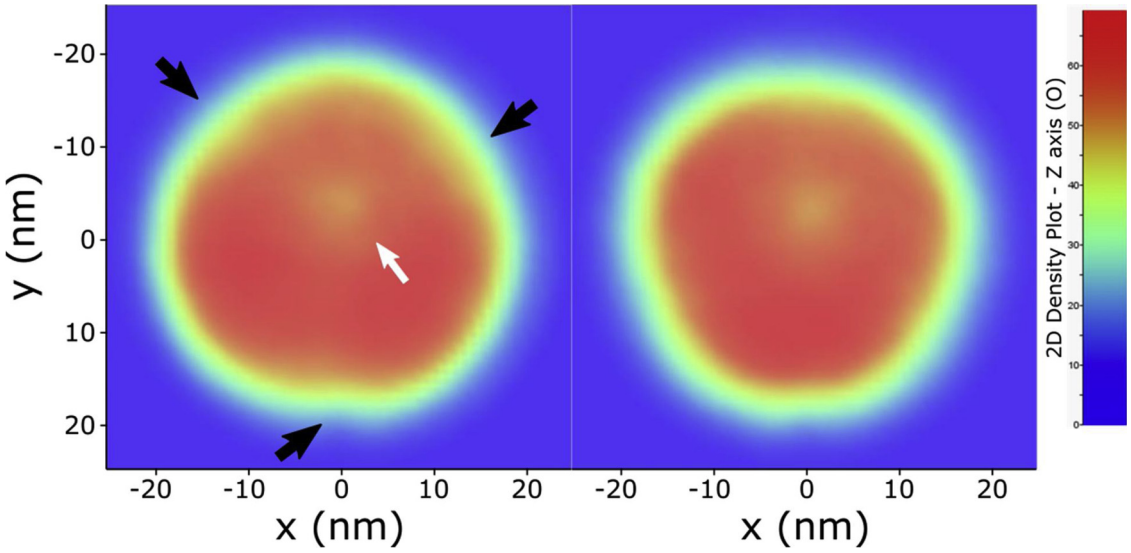

Fig. 6. 2D density plot in the x-y plane of oxygen atoms of spinel (100) plane on the left and (111) plane on the right). One low density pole (white arrow) and three low density lines (black arrows) are depicted in each image. Poles correspond to low order crystallographic planes (major crystallographic directions) where high electric field gradients exist. Similarly, zone lines have high fields and low atomic densities. The different position of the low-density areas in the two images points to a crystallography dependence of the atomic distribution pattern (i.e. distribution of the surface electric field).

Acknowledgements

This research was funded by the U.S. National Science Foundation (NSF), grant number EAR-1647012. Authors acknowledge the help of Drs. George E. Harlow (AMNH) and Dr. Harold Stowell (UA) in searching for the suitable samples and the American Museum of Natural History (Dept. of Earth and Planetary Sciences) for providing the spinel crystal. Authors also thank the two anonymous reviewers and the journal editorial board member, R.F. Egerton, whom suggestions greatly improved the quality of the final version of the manuscript.

Appendix A. Supplementary data

Supplementary material related to this article can be found, in the online version, at doi:https://doi.org/10.1016/j.micron.2020.102910.

References

Bachhav, M., Danoix, F., Hannoyer, B., Bassat, J.M., Danoix, R., 2013. Investigation of O-18 enriched hematite (α-Fe2O3) by laser assisted atom probe tomography. Int. J. Mass Spectrom. 335, 57–60.

Blavette, D., Sauvage, X., 2016. Chapter one - early developments and basic concepts. In: Lefebvre-Ulrikson, W., Vurpillot, F., Sauvage, X. (Eds.), Atom Probe Tomography. Academic Press, pp. 1–15.

Bunney, K., Freeman, S., Ogden, M.I., Richmond, W.R., Rohl, A.L., Jones, F., 2014. Effect of Lanthanum on the crystal growth of barium sulfate. Cryst. Growth Des. 14, 1650–1658.

Bunton, J.H., Olson, J.D., Lenz, D.R., Kelly, T.F., 2007. Advances in pulsed-laser atom probe: instrument and specimen design for optimum performance. Microsc. Microanal. 13, 418–427.

Danyushevsky, L., Robinson, P., Gilbert, S., Norman, M., Large, R., McGoldrick, P., Shelley, M.J.G.E., Environment, Analysis, 2011. Routine quantitative multi-element analysis of sulphide minerals by laser ablation ICP-MS: standard development and consideration of matrix effects. Geochem. Explor. Environ. Anal. 11, 51–60.

De Geuser, F., Gault, B., Bostel, A., Vurpillot, F., 2007. Correlated field evaporation as seen by atom probe tomography. Surf. Sci. 601, 536–543.

Devaraj, A., Colby, R., Hess, W.P., Perea, D.E., Thevuthasan, S., 2013. Role of photo-excitation and field ionization in the measurement of accurate oxide stoichiometry by laser-assisted atom probe tomography. J. Phys. Chem. Lett. 4, 993–998.

Diercks, D.R., Gorman, B.P., Kirchhofer, R., Sanford, N., Bertness, K., Brubaker, M., 2013. Atom probe tomography evaporation behavior of C-axis GaN nanowires: crystallographic, stoichiometric, and detection efficiency aspects. J. Appl. Phys. 114, 184903.

Eiler, J.M., Graham, C., Valley, J.W., 1997. SIMS analysis of oxygen isotopes: matrix effects in complex minerals and glasses. Chem. Geol. 138, 221–244.

Fougerouse, D., Reddy, S.M., Saxey, D.W., Erickson, T.M., Kirkland, C.L., Rickard, W.D.A., Seydoux-Guillaume, A.M., Clark, C., Buick, I.S., 2018. Nanoscale distribution of Pb in monazite revealed by atom probe microscopy. Chem. Geol. 479, 251–258.

Gault, B., Moody, M.P., Cairney, J.M., Ringer, S.P., 2012. Atom Probe Microscopy. Springer Science & Business Media.

Gordon, L.M., Tran, L., Joester, D., 2012. Atom probe tomography of apatites and bone-type mineralized tissues. ACS Nano 6, 10667–10675.

Huberty, J.M., Kita, N.T., Kozdon, R., Heck, P.R., Fournelle, J.H., Spicuzza, M.J., Xu, H., Valley, J.W., 2010. Crystal orientation effects in δ18O for magnetite and hematite by SIMS. Chem. Geol. 276, 269–283.

Kelly, T.F., Panitz, J.A., 2017. The first fifty years of atom probe. Micros. Today 25, 12–17.

Kita, N.T., Huberty, J.M., Kozdon, R., Beard, B.L., Valley, J.W., 2011. High-precision SIMS oxygen, sulfur and iron stable isotope analyses of geological materials: accuracy, surface topography and crystal orientation. SIMS Proceedings Papers 43, 427–431.

Kozdon, R., Kita, N.T., Huberty, J.M., Fournelle, J.H., Johnson, C.A., Valley, J.W., 2010. In situ sulfur isotope analysis of sulfide minerals by SIMS: precision and accuracy, with application to thermometry of ~3.5Ga Pilbara cherts. Chem. Geol. 275, 243–253.

La Fontaine, A., Piazolo, S., Trimby, P., Yang, L., Cairney, J.M., 2017. Laser-assisted atom probe tomography of deformed minerals: a zircon case study. Microsc. Microanal. 23, 404–413.

Larson, D.J., Gault, B., Geiser, B.P., De Geuser, F., Vurpillot, F., 2013a. Atom probe tomography spatial reconstruction: status and directions. Curr. Opin. Solid State Mater. Sci. 17, 236–247.

Larson, D.J., Prosa, T., Ulfig, R.M., Geiser, B.P., Kelly, T.F.J.N.Y., 2013b. Local Electrode Atom Probe Tomography. US: Springer Science.

Mancini, L., Amirifar, N., Shinde, D., Blum, I., Gilbert, M., Vella, A., Vurpillot, F., Lefebvre, W., Lardé, R., Talbot, E., Pareige, P., Portier, X., Ziani, A., Davesnne, C., Durand, C., Eymery, J., Butté, R., Carlin, J.-F., Grandjean, N., Rigutti, L., 2014. Composition of wide bandgap semiconductor materials and nanostructures measured by atom probe tomography and its dependence on the surface electric field. J. Phys. Chem. C 118, 24136–24151.

Miller, M.K., Russell, K.F., Thompson, K., Alvis, R., Larson, D.J., 2007. Review of atom probe FIB-Based specimen preparation methods. Microsc. Microanal. 13, 428–436.

Morris, J.H.R., Cuduvally, R., Melkonyan, D., Fleischmann, C., Zhao, M., Arnoldi, L., van der Heide, P., Vandervorst, W., 2018. Toward accurate composition analysis of GaN and AlGaN using atom probe tomography. Journal of Vacuum Science & Technology B 36 03F1301-1303F1306.

Morris, J.H.R., Cuduvally, R., Melkonyan, D., Zhao, M., van der Heide, P., Vandervorst, W., 2019. Atom probe of GaN/AlGaN heterostructures: the role of electric field, sample crystallography and laser excitation on quantification. Ultramicroscopy 206, 112813.

Ottolini, L., Cámara, F., Hawthorne, F.C., Stirling, J., 2002. SIMS matrix effects in the analysis of light elements in silicate minerals: comparison with SREF and EMPA data. Am. Mineral. 87, 1477–1485.

Paquette, J., Reeder, R.J., 1995. Relationship between surface structure, growth mechanism, and trace element incorporation in calcite. Geochim. Cosmochim. Acta 59, 735–749.

Pérez-Huerta, A., Laiginhas, F., Reinhard, D.A., Prosa, T.J., Martens, R.L., 2016. Atom probe tomography (APT) of carbonate minerals. Micron 80, 83–89.

Reddy, S.M., Saxey, D.W., Rickard, W.D.A., Fougerouse, D., Montalvo, S.D., Verberne, R., van Riessen, A., 2020. Atom probe tomography: development and application to the geosciences. Geostand. Geoanalytical Res. 44, 5–50.

Reeder, R.J., Rakovan, J., 1999. Surface structural controls on trace element

incorporation during crystal growth. In: Jamtveit, B., Meakin, P. (Eds.), Growth, Dissolution and Pattern Formation in Geosystems. Springer, Netherlands, Dordrecht, pp. 143–162.
Riley, J.R., Bernal, R.A., Li, Q., Espinosa, H.D., Wang, G.T., Lauhon, L.J., 2012. Atom probe tomography of a-Axis GaN nanowires: analysis of nonstoichiometric evaporation behavior. ACS Nano 6, 3898–3906.
Saxey, D.W., 2011. Correlated ion analysis and the interpretation of atom probe mass spectra. Ultramicroscopy 111, 473–479.
Saxey, D.W., Moser, D.E., Piazolo, S., Reddy, S.M., Valley, J.W., 2018. Atomic worlds: current state and future of atom probe tomography in geoscience. Scr. Mater. 148, 115–121.
Śliwiński, M.G., Kitajima, K., Kozdon, R., Spicuzza, M.J., Fournelle, J.H., Denny, A., Valley, J.W., 2016. Secondary ion mass spectrometry Bias on isotope ratios in Dolomite–Ankerite, Part I: δ18O. Matrix Effects. 40, 157–172.
Śliwiński, M.G., Kitajima, K., Spicuzza, M.J., Orland, I.J., Ishida, A., Fournelle, J.H., Valley, J.W., 2018. SIMS Bias on Isotope Ratios in Ca-Mg-Fe Carbonates (Part III): δ18O and δ13C Matrix Effects Along the Magnesite–Siderite Solid-Solution Series. Wiley Online Library 42, 49–76.
Sylvester, P., 2008. Matrix Effects in Laser Ablation ICP-MS, Laser Ablation ICP-MS in the Earth Sciences: Current Practices and Outstanding Issues. Mineralogical Association of Canada, pp. 67–78.
Valley, J.W., Kita, N.T., 2009. In situ Oxygen Isotope Geochemistry by Ion Microprobe, MAC Short Course: Secondary Ion Mass Spectrometry in the Earth Sciences. pp. 19–63.
Weber, J., Barthel, J., Brandt, F., Klinkenberg, M., Breuer, U., Kruth, M., Bosbach, D., 2016. Nano-structural features of barite crystals observed by electron microscopy and atom probe tomography. Chem. Geol. 424, 51–59.
Wingate, M.T.D., Compston, W., 2000. Crystal orientation effects during ion microprobe U–Pb analysis of baddeleyite. Chem. Geol. 168, 75–97.
Yao, L., Gault, B., Cairney, J.M., Ringer, S.P., 2010. On the multiplicity of field evaporation events in atom probe: a new dimension to the analysis of mass spectra. Philos. Mag. Lett. 90, 121–129.